ACS APPLIED MATERIALS & INTERFACES

Research Article

www.acsami.org

Morphology and Interfacial Energetics Controls for Hierarchical Anatase/Rutile TiO_2 Nanostructured Array for Efficient Photoelectrochemical Water Splitting

Jih-Sheng Yang, Wen-Pin Liao, and Jih-Jen Wu*

Department of Chemical Engineering, National Cheng Kung University, Tainan 701, Taiwan

Supporting Information

ABSTRACT: In this work, a three-dimensional (3D) hierarchical TiO_2 nanostructured array is constructed on the basis of the considerations of morphology and interfacial energetics for photoelectrochemical water splitting. The photoelectrode is composed of a core−shell structure where the core portion is a rutile TiO_2 nanodendrite (ND) array and the shell portion is rutile and anatase TiO_2 nanoparticles (NPs) sequentially located on the surface. The TiO_2 ND array provides a fast electron transport pathway due to its quasi-single-crystalline structure. The 3D configuration with NPs in the shell portion provides a larger surface area for more efficient photocharge separation without significantly sacrificing the electron collection efficiency. Moreover, anatase TiO_2 NPs constructed on the surface of the ND/rutile TiO_2 NP nanostructured array enhance charge separation and suppress charge recombination at the interfacial region due to the higher conduction band edge of anatase TiO_2 compared to that of rutile TiO_2. A photocurrent density and photoconversion efficiency of 2.08 mA cm^{-2} at 1.23 V vs reversible hydrogen electrode (RHE) and 1.13% at 0.51 V vs RHE are, respectively, attained using the hierarchical TiO_2 nanostructured array photoelectrochemical cell under illumination of AM 1.5G (100 mW cm^{-2}).

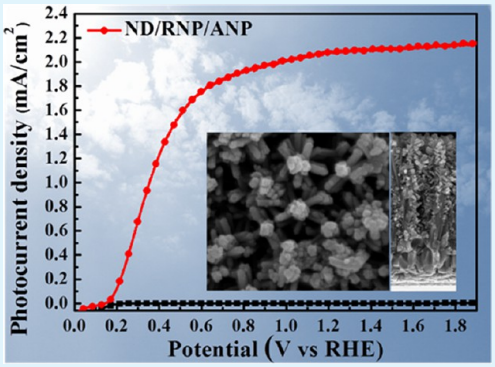

KEYWORDS: *hierarchical nanostructures, solar energy, titanium dioxide, photocatalysis, water splitting*

INTRODUCTION

Solar light, which is the most abundant renewable energy source, can be stored in the form of chemical bonds for the practical utilization of solar energy. Efficient conversion of the energy harvested from sunlight into chemical fuel in the simplest chemical bond of H_2 can be conducted using a photoelectrochemical (PEC) water splitting cell. A PEC cell, demonstrated by Honda and Fujishima,[1] is composed of a TiO_2 photoelectrode and a Pt counter electrode. When sunlight irradiates the TiO_2 photoelectrode, the photogenerated electrons reduce water to form H_2 on the Pt counter electrode and holes oxidize water to produce O_2 on the TiO_2 electrode with some external bias. Studies on PEC cells have mainly focused on evaluating new semiconductors for fabricating efficient and stable photoanodes with appropriate bandgap and band-edge positions, low electrical resistance, and suitable chemical stability and photocorrosion resistance.[2−4] Nevertheless, TiO_2 is still one of the most attractive photocatalysts because of its low-cost, stability, and nontoxicity. Narrowing of the TiO_2 band gap has been successfully demonstrated by compositional doping[5] and hydrogenation[6] to enhance visible light absorption.

The utilization of nanoparticle (NP)-film photoelectrodes for solar hydrogen conversion has been intensively investigated.[7] NP-film photoelectrodes, which consist of small grains, have large surface-area-to-volume ratios and reduce the distance for photogenerated holes migrating to active sites on the surface. However, the electron transport rate in NP films is much lower than that in a bulk single crystal due to the large number of trap states at grain boundaries, resulting in significant charge recombination in NP-film photoelectrodes. Crystalline TiO_2 exists in one of three structures: anatase, rutile, and brookite.[8] By coupling anatase and rutile TiO_2 NPs, a crystalline phase-dependent synergistic effect has been reported during photocatalytic H_2 production from aqueous methanol, but the effect is absent during PEC measurements.[9] The synergistic effect results from the slightly lower conduction band edge of the rutile phase, which allows the transfer of photoelectrons from the anatase to rutile phases, suppressing photocharge recombination. However, it has been suggested that the applied potential during PEC water reduction may render the interparticle charge separation less important.[9]

The utilization of one-dimensional (1D) nanostructured (nanotube (NT), nanorod (NR), and nanowire (NW) array) photoelectrodes in PEC water splitting cells has received increasing attention.[10−15] Unlike NP-film photoelectrodes,

Received: May 9, 2013
Accepted: July 11, 2013
Published: July 11, 2013

these photoelectrodes exhibit direct and ordered channels for electron transport to the collecting electrodes. With vertically aligned 1D features, light absorption and minority charge diffusion paths can be decoupled to different directions to enhance photocharge collection efficiency.[3] For anatase TiO_2, the optical path length required for a light harvest of 90% is about 1 μm and the hole diffusion length is about 70 nm.[11] A pristine TiO_2 PEC water splitting with encouraging performance was attained using TiO_2 NT arrays by tuning the morphology of the hierarchical nanostructures.[12] The photocurrent density and photoconversion efficiency of the TiO_2 NT-array PEC cell are 1.59 mA cm^{-2} at 1.23 V vs reversible hydrogen electrode (RHE) and 0.84% under illumination of AM 1.5G, respectively.[12] Single-crystalline NR and NW arrays have high electron mobility and are thus expected to exhibit superior PEC water splitting performance. Branched rutile TiO_2 NR arrays, which have better charge transport than that of NP film and larger surface area for more efficient photocharge collection than that of bare NR arrays, have demonstrated a promising photocurrent density of 0.83 mA cm^{-2} at 0.8 V vs RHE under illumination of AM 1.5G (88 mW cm^{-2}).[13]

The photoconversion efficiency (η) of a PEC cell can be considered as the product of light harvesting efficiency(η_{LH}), charge separation efficiency (η_s), and charge collection efficiency (η_c):

$$\eta = \eta_{LH} \cdot \eta_s \cdot \eta_c \quad (1)$$

In this work, a three-dimensional (3D) hierarchical TiO_2 nanostructured array is constructed on the basis of the considerations of morphology and interfacial energetics to serve as an efficient PEC photoelectrode. The photoelectrode is composed of a core−shell structure. The core portion is a rutile TiO_2 nanodendrite (ND) array, and the shell portion is rutile and anatase TiO_2 NPs sequentially located on the surface. A light harvest of more than 95% in the range of 300−375 nm is achieved using the hierarchical TiO_2 nanostructured photoelectrode with a thickness of ~2 μm. The TiO_2 ND array provides a fast electron transport pathway due to its quasi-single-crystalline structure. The 3D configuration with NPs in the shell portion provides a larger surface area for more efficient photocharge separation without significantly sacrificing the electron collection efficiency. Moreover, anatase TiO_2 NPs (ANPs) constructed on the surface of the ND/rutile TiO_2 NP (RNP) nanostructured array enhance charge separation and suppress charge recombination at the interfacial region due to the higher conduction band edge of anatase TiO_2 compared to that of rutile TiO_2. With a large surface area, high charge recombination resistance, and a fast electron transport rate, a photocurrent density and photoconversion efficiency of 2.08 mA cm^{-2} at 1.23 V vs RHE and 1.13% at 0.51 V vs RHE are, respectively, attained using the hierarchical TiO_2 nanostructured array PEC cell under illumination of AM 1.5G.

EXPERIMENTAL SECTION

Aligned TiO_2 NW arrays were hydrothermally grown on a seeded fluorine-doped tinoxide (FTO) substrate[16] by a two-batch method. The first batch was carried out in a solution of 40 mL of 8 M hydrochloric acid in deionized water and 0.75 mL of titanium(IV) *tert-n*-butoxide (TnBT) (solution A) at 150 °C for 3.5 h. The second batch of the hydrothermal process was conducted at 150 °C for 10 h using a solution of 40 mL of 8 M hydrochloric acid in saturated NaCl solution and 0.75 mL of TnBT. The seed layer was prepared by immersing the FTO substrate in 0.05 M aqueous solution of $TiCl_4$ at 50 °C for 1 h followed by heat treatment at 450 °C for 30 min. To further develop NDs from the NW array, chemical bath deposition of the sprout-like nanostructures on the TiO_2 NWs was first conducted in a solution of 40 mL of 0.25 M HCl and 1 mL of titanium(IV) *tert*-isopropoxide at 95 °C for 4 h. Another 1.5 h hydrothermal process in solution A at 150 °C was subsequently carried out to elongate the sprouts for the formation of branches on the TiO_2 NWs. To synthesize RNPs on the surface of the ND and NW arrays, the array/FTO substrate was immersed in an aqueous solution of 0.1 M $TiCl_4$ at 50 °C for 1 h followed by heat treatment at 450 °C for 30 min. The formation of ANPs on the rutile TiO_2 nanostructures was conducted via a solvothermal method using 1 mL of TnBT mixed with 40 mL of 1-butanol solution of 3.5 M acetic acid at 200 °C for 12 h.

The morphologies of the nanostructures were examined using scanning electron microscopy (SEM) (JEOL JSM-7000F). Structural characterizations of the hierarchical anatase/rutile TiO_2 nanostructures were performed using transmission electron microscopy (TEM) (FEI E.O Tecnai F20 G2MAT S-TWIN). Optical absorptions of the TiO_2 nanostructured arrays were measured using an ultraviolet−visible-infrared (UV−vis-IR) spectrophotometer (JASCO V-670). The PEC performance of the TiO_2 nanostructured arrays was examined using a three-electrode system with a supporting electrolyte of 1 M KOH solution under simulated sunlight illumination at 100 mW cm^{-2} from a 300-W xenon lamp (Newport 66983) coupled with an AM 1.5G filter (Newport 81094). The TiO_2 nanostructured arrays were fabricated into photoelectrodes with a well-defined area of 1 cm^2. The TiO_2 nanostructured photoelectrodes, Pt foil, and a nonaqueous Hg/HgO electrode (0.098 V vs normal hydrogen electrode (NHE) at 25 °C) were used as the working, counter, and reference electrodes, respectively. Electrochemical impedance spectroscopy (EIS) measurements were carried out under an illumination of AM 1.5 (100 mW cm^{-2}) by applying a 10 mV AC signal over the frequency range of 50 mHz to 100 kHz at the open-circuit potential (OCPs) of the PEC cells using a potentiostat with a frequency response analyzer (FRA) (Autolab, PGSTAT30 and FRA2 module).

RESULTS AND DISCUSSION

Hierarchical anatase/rutile TiO_2 nanostructured arrays were constructed on FTO substrate using a wet chemical route. Figure 1a,b shows top-view and cross-sectional-view SEM images of the ND/RNP/ANP array, respectively. They confirm that 3D networks formed on the FTO substrate. The quasi-singlecrystalline structure of the rutile ND was demonstrated in our previous work.[16] To further examine the hierarchical configuration of the TiO_2 nanostructure, high-resolution transmission electron microscopy (HRTEM) was employed to investigate the crystal structures of the RNPs and ANPs grown on single-crystalline NWs in sequence. As shown in Figure 1c, RNPs with diameters of 2−3 nm formed on the surface of the 1D single-crystalline rutile nanostructure followed by ANPs with diameters of 1.3−7.0 nm on the shell of the hierarchical nanostructure. The formations of RNPs and ANPs on the rutile NW arrays are also confirmed by Raman spectroscopy, as shown in Figure S1 (Supporting Information). For comparison, 2-μm-thick TiO_2 nanostructured arrays with NW, NW/RNP, NW/RNP/ANP, and ND/RNP/ANP configurations, respectively, were employed as photoelectrodes in PEC cells for water splitting. Typical SEM images of NW, NW/RNP, and NW/RNP/ANP arrays are shown in Figure S2 (Supporting Information).

Absorption spectra of the TiO_2 nanostructured arrays obtained from the relation of (1 − total transmittance (T) − total reflectance (R)) are shown in Figure 2. Incident light with wavelengths in the range of 300−375 nm was almost totally absorbed by the 2 μm-thick rutile TiO_2 NW array. When the RNPs and ANPs hierarchically form on the TiO_2 NW array in sequence, the diffuse reflectance is slightly enhanced, as shown

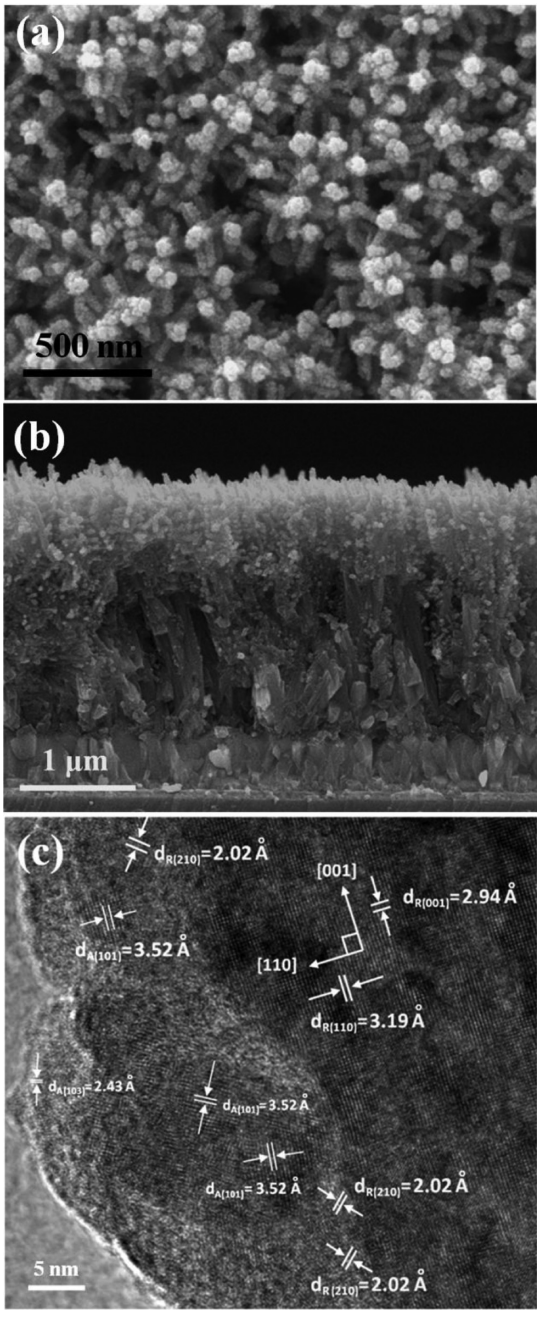

Figure 1. (a) Top-view and (b) cross-sectional-view SEM images of TiO_2 ND/RNP/ANP arrays. (c) HRTEM image of TiO_2 NW/RNP/ANP.

in the inset of Figure 2, due to the light scattering effect from the increased surface roughness.[13] Absorptions $(1 - R - T)$ of NW/RNP and NW/RNP/ANP arrays are therefore slightly reduced by ~1%. A ~4% reduction in the ultraviolet (UV) absorption was observed in the ND/RNP/ANP array as a result of light scattering, as shown in Figure 2. The light absorption measurements indicate that the UV-light harvest efficiencies of the TiO_2 nanostructured arrays is not enhanced by hierarchically growing NPs and by constructing a 3D configuration on the NW arrays even though the volumes of the TiO_2 nanostructures are increased. It should be noted that the shell portion of the anatase/rutile NPs should be efficiently excited by the illumination since the light is incident from the top side of the hierarchical TiO_2 nanostructure to the FTO substrate.

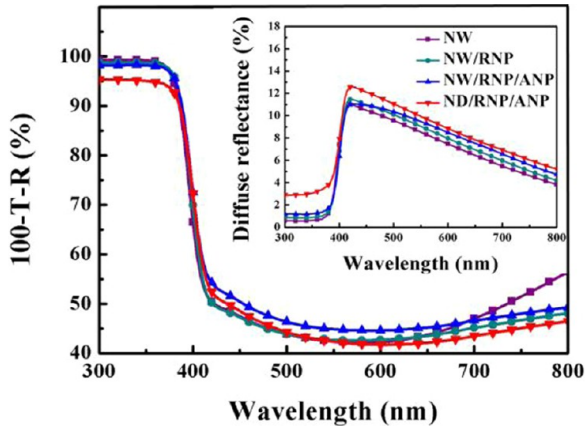

Figure 2. Absorption spectra and diffuse reflectance spectra (inset) of the TiO_2 nanostructured arrays.

Figure 3a shows the photocurrent density (J)−potential (V) curves of the TiO_2 nanostructured arrays obtained by linear sweep photovoltammetry measurements using a three-electrode electrochemical configuration in 1 M KOH electrolyte under AM 1.5G (100 mW cm^{-2}) illumination. For comparison, the J−V curve of P25 film is also shown in the figure. The photocurrent densities of the P25 NP film, NW, NW/RNP, NW/RNP/ANP, and ND/RNP/ANP are 0.03, 0.03, 0.92, 1.60, and 2.08 mA cm^{-2}, respectively, at 1.23 V vs RHE. Compared to the P25 NP film, the NW array has a similar low photocurrent density whereas the NW/RNP array has a significantly higher photocurrent density for applied potentials larger than the OCP of 0.2 V vs RHE. When ANPs are grown on the surface of NW/RNP, as shown in Figure 3a, a steeper increase in current with respect to potential and a significantly enhanced saturation photocurrent density are observed in the J−V curve of the NW/RNP/ANP photoanode. With the slightly lower light harvesting efficiency, as shown in Figure 2, the NW/RNP/ANP photoelectrode exhibits superior PEC water splitting performance compared to that of the NW/RNP photoelectrode. The photocatalytic performance of the rutile/antanse TiO_2 nanostructure is further increased by constructing the 3D configuration of the ND/RNP/ANP photoelectrode, although the light harvest efficiency of the ND/RNP/ANP array is slightly inferior to that of the NW/RNP/ANP array.

The photoconversion (photon-to-hydrogen) efficiency (η) of the TiO_2 photoelectrodes was estimated using the equation:[15]

$$\eta\ (\%) = [J_{ph}(1.23 - V_{appl})/P_{total}] \times 100\% \quad (2)$$

where J_{ph} is the photocurrent density at a bias V_b vs RHE, V_{appl} is the potential difference between V_b and E^o (H_2O/H_2) (= −0.0146 V vs RHE in a 1.0 M KOH solution), and P_{total} is the incident light intensity (= 100 mW cm^{-2}). The plots of the photoconversion efficiency for the TiO_2 nanostructured arrays as a function of applied bias are illustrated in Figure 3b. The maximum η for the NW/RNP array is 0.44% at 0.56 V vs RHE. With ANPs on the surface, the maximum η for the NW/RNP/ANP array is significantly increased to 0.86% at 0.5 V vs RHE. Moreover, the maximum η for TiO_2 is further enhanced to 1.13% (at 0.51 V vs RHE) by constructing a 3D nanostructured configuration of ND/RNP/ANP.

Figure 3c shows the incident photon-to-current conversion efficiency (IPCE) of the TiO_2 nanostructured arrays measured

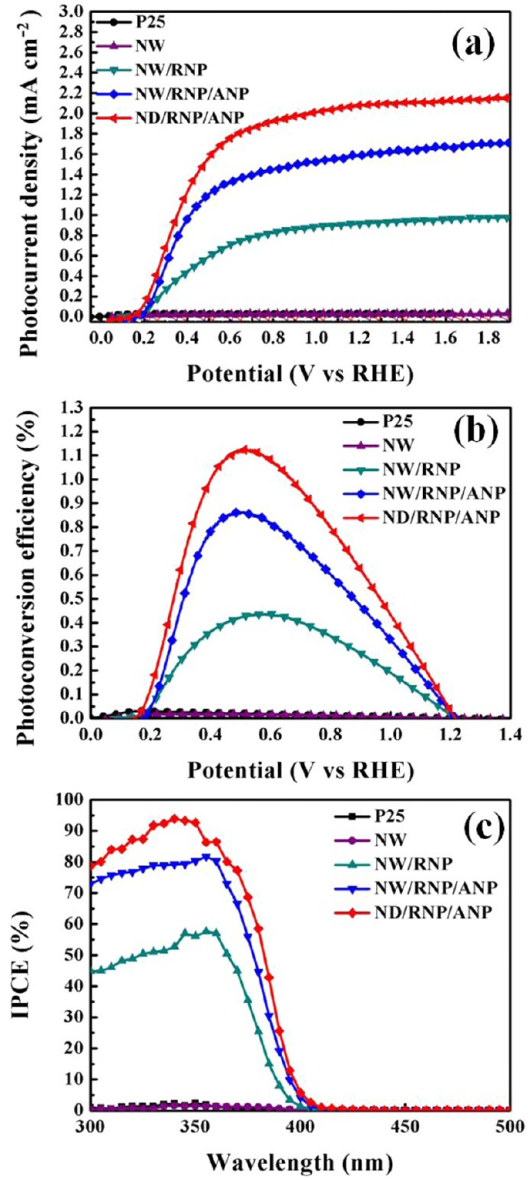

Figure 3. PEC properties of TiO_2 nanostructured arrays. (a) $J-V$ curves obtained with a scan rate of 5 mVs^{-1}. (b) Photoconversion efficiency as a function of the applied potential. (c) IPCE spectra measured at an applied bias of 0.6 V vs RHE.

at 0.6 V vs RHE. It reveals that the three TiO_2 nanostructured arrays have significantly improved IPCE values over the entire UV region compared to those of P25 NP film and NW array. At wavelengths shorter than 360 nm, the IPCE values of the NW/RNP and NW/RNP/ANP arrays are 45−57% and 73−81%, respectively. The ND/RNP/ANP array exhibits the highest IPCE values of 78−93% among the three TiO_2 nanostructured arrays, which is consistent with the results of $J-V$ measurements. The IPCE values of the three TiO_2 nanostructured arrays are negligible at wavelengths longer than 410 nm, which matches with the band gap energy (3.0 eV) of rutile TiO_2. It indicates that the rutile nanostructures contribute to photocurrents in the NW/RNP/ANP and ND/RNP/ANP arrays.

The photoresponse of the three TiO_2 nanostructured arrays over time was measured at an applied potential of 1.5 V vs RHE under chopped AM 1.5G illumination. As shown in Figure 4, fast photoresponses were demonstrated in the three TiO_2

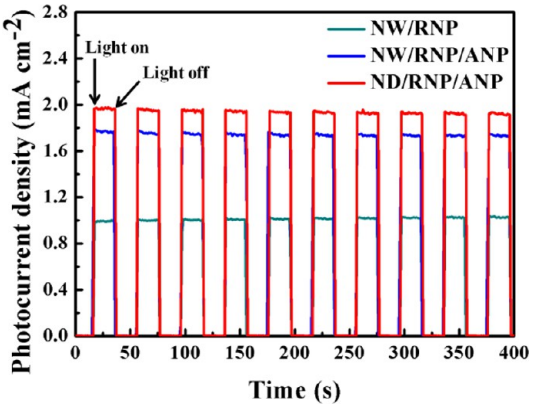

Figure 4. $J-t$ curves at an applied potential of 1.5 V vs RHE under illumination with 60 s light on/off cycles.

nanostructured arrays. A constant photocurrent density without decay is obtained from the light-on period of each cycle, indicating that the $J-t$ patterns of light on/off cycles are highly reproducible for the three photoelectrodes. Among the three TiO_2 nanostructured arrays, the ND/RNP/ANP photoelectrode had the highest photocurrent density in the light-on period, consistent with Figure 3a.

The photocurrent decay to a steady-state photocurrent density, in the time scales of ∼ms to ∼s, is typically observed in a PEC cell after irradiation is suddenly switching on.[10,17−19] The photocurrent decay is mainly attributed to holes trapped at surface states recombining with electrons from the conduction band.[20] To examine this photocurrent transient behavior of the TiO_2 nanostructured arrays, the $J-t$ measurements were conducted at applied potentials slightly higher than OCP, i.e., 0.3 V vs RHE, under chopped AM 1.5G illumination, as shown in Figure5a. Significant photocurrent decay occurs in the $J-t$ curve of the NW photoelectrode. The photocurrent decay is substantially reduced in the $J-t$ curve of the NW/RNP photoelectrode. Constant photocurrent densities without decay are obtained in the $J-t$ curves of the NW/RNP/ANP and ND/RNP/ANP photoelectrodes. The results indicate that the recombination of holes trapped at surface states with electrons from the conduction band is gradually suppressed once RNPs and ANPs form on the NW surface in sequence.

When performing water splitting using a UV-irradiated TiO_2 photoelectrode, the photogenerated electrons reduce water to form H_2 on the Pt counter electrode and holes oxidize water to produce O_2 on the TiO_2 electrode with some external bias. Electron transport in the photoelectrode and interface charge transfer from the photoelectrode to water play crucial roles in the water-splitting efficiency of PEC cells. In the present work, EIS was employed to analyze the carrier dynamics in the PEC cells with TiO_2 nanostructured electrodes for water splitting. Figure 5b shows Nyquist plots of the impedance data of the PEC cells measured at OCP under AM 1.5G (100 mW cm^{-2}) illumination. An equivalent circuit representing the PEC cell, shown in the inset of Figure 5b, based on the diffusion-recombination model[21] was employed for analyzing the EIS spectra (Supporting Information). The characteristic times of electron transport through the photoelectrode (τ_t) and charge transfer at the interface (τ_c) estimated from the impedance analyses are listed in Table 1. The electron collection efficiency (η_c) at OCP calculated from the relation $\eta_c = 1 - (\tau_t/\tau_c)$[22] is also displayed in Table 1.

dx.doi.org/10.1021/am401746b | ACS Appl. Mater. Interfaces 2013, 5, 7425−7431

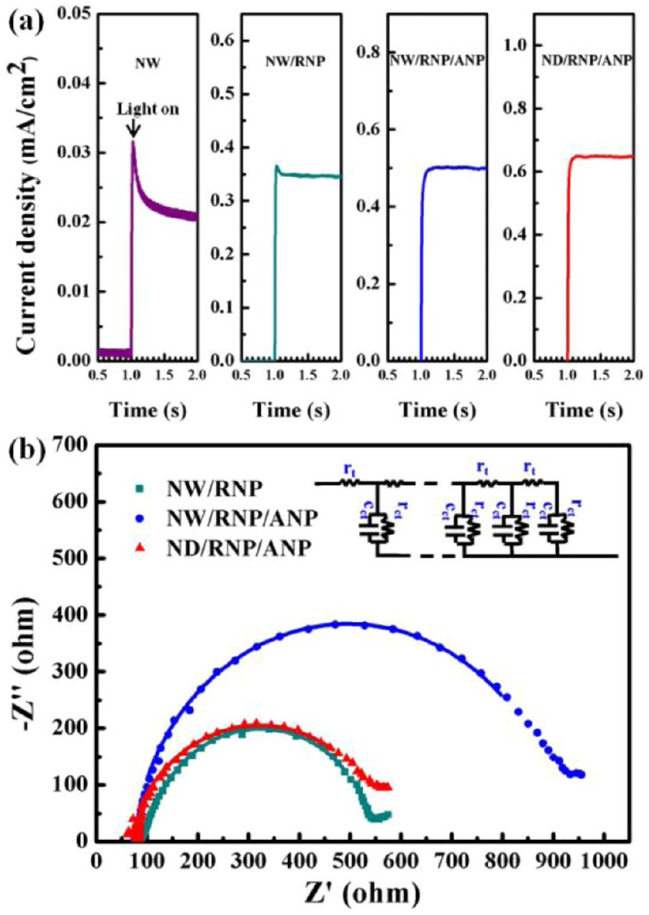

Figure 5. (a) Photocurrent transient behavior of TiO_2 nanostructured photoelectrodes in response to on−off irradiation. (b) Nyquist plots of PEC cells measured at OCP under AM 1.5G (100 mW cm^{-2}) illumination. The solid lines are the fitting results based on the equivalent circuit model shown in the inset, where C_{ct} is the chemical capacitance, r_{ct} is the charge-transfer resistance related to recombination of an electron, and r_t is the electron transport resistance.

Table 1. Characteristic Times of Electron Transport through the Photoelectrode (τ_t) and Charge Transfer at the Interface (τ_c) and Electron Collection Efficiency of TiO_2 Nanostructured Photoelectrodes

cell	τ_t (ms)	τ_c (ms)	η_c (%)
NW/RNP	1.1	106	99
NW/RNP/ANP	2.8	311	99
ND/RNP/ANP	10.2	354	97

As shown in Table 1, the τ_c values for the three TiO_2 nanostructured photoelectrodes are on the time scale of ∼hundreds of ms. It has been reported that the photogenerated holes on bare TiO_2 oxidize water within 2 μs.[23] Time-resolved infrared (IR) absorption measurements indicate that holes reacted with surface hydroxyls within 2 μs, and the recombination decay of the photoelectrons in TiO_2 is obstructed in the presence of water vapor.[24] In this work, EIS was conducted over the frequency range of 50 mHz−100 kHz, which cannot resolve the short characteristic time for the oxidation of water on the TiO_2 surface by photogenerated holes. Moreover, the water could not consume the photoelectrons based on time-resolved IR absorption measurements.[24] Therefore, the corresponding process of interface charge transfer extracted from the EIS data with the characteristic times of ∼hundreds of ms may be the reduction of photogenerated oxidized species in water by the electrons in the conduction band of TiO_2.[20,25] Such TiO_2/water interfacial reaction, which consumes the photogenerated electrons, decreases the number of electrons transported to the Pt counter electrode for H_2 production. In this aspect, the characteristic time τ_c also reflects the electron lifetime in the photoelectrode under the flat band condition of OCP.

The τ_c value for the NW/RNP/ANP photoelectrode is prolonged by 3-fold compared to that for the NW/RNP photoelectrode, as listed in Table 1. A comparable τ_c value is also obtained for the ND/RNP/ANP photoelectrode. Compared to the NW/RNP PEC cells, the poor charge transfer characteristic observed in the NW/RNP/ANP and ND/RNP/ANP PEC cells indicates less interfacial recombination between the ANP-covered photoelectrodes and water under the OCP condition. The results show that the electron lifetime in the TiO_2 nanostructured photoelectrode is strongly influenced by the crystal structure and configuration of the photoelectrode. The electron lifetime is enhanced by the formation of ANPs on the surface of the rutile TiO_2 nanostructured photoelectrode.

The τ_t values for the three TiO_2 nanostructured PEC cells were extracted from the EIS data, as listed in Table 1. The τ_t value at OCP increased when ANPs formed on the NW/RNP. The τ_t value for the ND/RNP/ANP photoelectrode increased compared to that for the NW/RNP/ANP photoelectrode. Nevertheless, the τ_t values for the hierarchical TiO_2 nanostructured photoelectrodes are significantly shorter than τ_c. As listed in Table 1, although the ND/RNP/ANP photoelectrode has a slightly lower η_c than those of the other two photoelectrodes, because of the slower electron transport rate, the η_c values for the three TiO_2 nanostructured PEC cells all approach 100%.

As shown in Figure 3, the NW/RNP photoelectrode outperforms the NW array in terms of PEC performance. This is mainly attributed to the alteration of the photoelectrode morphology by the RNPs, as shown in Figure S3 (Supporting Information). Since the thickness of the RNP layer on the surface of the NW array is less than the hole diffusion length (∼10 nm for sintered rutile TiO_2 electrode),[26] the large surface area created by NPs facilitates holes at the surface transferring from the active sites to water. It is confirmed by the results shown in Figure 5a that the photocurrent decay for the NW/RNP PEC cell is lower than that for the NW PEC cell. In addition to the advantages of the pristine NW array, including the decoupled hole diffusion path and fast electron transport rate, the conformal RNP layer improves the photogenerated-charge separation efficiency of the photoelectrode. It finally results in significant enhancements of the photocurrent density and efficiency of the PEC cell.

With the successful morphology control for the rutile NW/NP photoelectrode for improving charge separation, the modification of interfacial energetics is an additional strategy for further enhancing the performance of a PEC cell. It is achieved by the formation of a conformal ANP layer on the surface of NW/RNP and ND/RNP photoelectrodes, as shown in Figure 3. In general, the photocatalytic activity of anatase is superior to that of rutile TiO_2 although it is essentially complex to relate TiO_2 photocatalytic activity simply to crystal phase.[9] Since the valence band edges of the anatase and rutile phases are at the same potential,[9] the holes photogenerated within

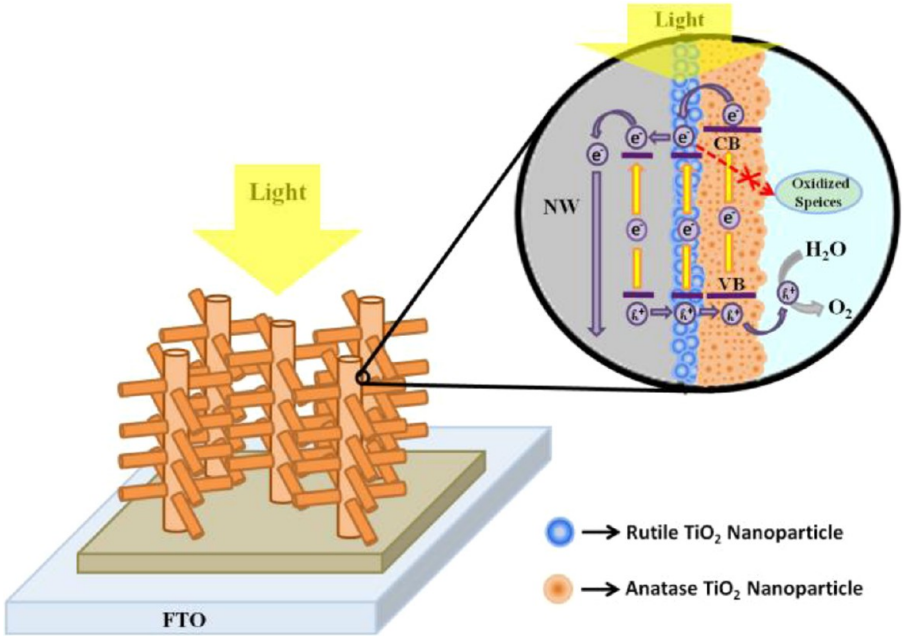

Figure 6. Schematic diagram illustrating the respective band positions and photogenerated charge separation in the hierarchical anatase/rutile TiO_2 nanostructured arrays.

NW/RNP/ANP and ND/RNP/ANP can efficiently transfer from the reaction sites of ANPs to water once the thickness of the ANP layer is less than the hole diffusion length. This is confirmed by IPCE results in Figure 3c that the rutile nanostructures contribute to photocurrents in the NW/RNP/ANP and ND/RNP/ANP arrays. Due to the higher conduction band edge of anatase TiO_2 compared to that of rutile TiO_2, the formation of ANPs on the surfaces of NW/RNP and ND/RNP arrays increases the band bending in the space charge regions of the photoelectrodes in contact with water under a given bias. The photogenerated electrons in the space charge regions of NW/RNP/ANP and ND/RNP/ANP photoelectrodes are sped up to the bulk electrode with the enlarged band bending. Due to the enhancements of charge separation from these two aspects by the interfacial energetics control, the surface recombination of the photogenerated charges is significantly reduced in the NW/RNP/ANP and ND/RNP/ANP photoelectrodes. Constant photocurrent densities are therefore observed from the photocurrent transient measurements of the NW/RNP/ANP and ND/RNP/ANP photoelectrodes, as shown in Figure 5a.

Moreover, EIS results show that the electron lifetime in the photoelectrode is enhanced by the formation of ANPs on the surface of the rutile TiO_2 nanostructured photoelectrode, as listed in Table 1. This may be attributed to the following reasons, also associated with the interfacial energetics. As shown in the scheme of Figure 6, in the absence of a space charge region under the flat band condition, the photogenerated electrons in the conduction band of the ANP layer prefer to transfer to that of the rutile nanostructure in the core of the photoelectrode due to the conduction band edge of anatase being higher than that of rutile. In addition, the ANP layer with higher conduction band edge also acts as a recombination barrier in the NW/RNP/ANP and ND/RNP/ANP PEC cells. As shown in Figure 6, in the presence of the recombination barrier (ANP layer), the electrons on the conduction band of the rutile nanostructure, which either come from ANPs or are generated by self-photoexcitation, are restricted to reacting with the photogenerated oxidized species in water. The electron lifetime in the photoelectrode is therefore enhanced.

The formation of the ANP layer creates more grain boundaries, which can increase the number of trapping centers for electrons. Compared to the NW/RNP photoelectrode, a slower electron transport rate in the NW/RNP/ANP photoelectrode is observed at OCP from EIS measurements due to more electron trapping/detrapping events occurring in the photoelectrodes. In this study, the number of ANPs on the ND/RNP/ANP array is larger than that on the NW/RNP/ANP array, as shown in Figure S4 (Supporting Information). With the larger number of ANPs, the electron transport time in the ND/RNP/ANP photoelectrode is therefore prolonged. It is worth noting that water splitting is normally performed at an applied bias rather than at the flat band condition of OCP in order to obtain photocurrent, in this case, the bend blending existing in the space charge region, where the shell portions of the ANPs and RNPs in the NW/RNP/ANP and ND/RNP/ANP photoelectrodes are located. Therefore, the electron detrapping process is enhanced at the PEC operating condition compared to that at the flat band condition during EIS measurements. As a result, the electron collection efficiency in the ND/RNP/ANP photoelectrode should be higher than that estimated at the flat band condition.

Although the light harvest efficiency of the ND/RNP/ANP array is slightly inferior to that of the NW/RNP/ANP array, the 3D configuration of the ND/RNP/ANP photoelectrode provides a larger surface area, which facilitates the photogenerated holes more efficiently transferring to water and producing O_2. The charge separation efficiency and therefore the photocurrent density of the PEC cell are increased with the 3D hierarchical TiO_2 photoelectrode under a given illumination. Through both morphology and interfacial energetics controls, a PEC photoelectrode with high charge separation efficiency, long electron lifetime, and fast electron transport rate

is attainable. A notable photocurrent density for PEC water splitting is therefore achieved using the 3D hierarchical anatase/rutile TiO_2 nanostructured array.

CONCLUSIONS

A 3D hierarchical TiO_2 nanostructured array composed of a ND/RNP/ANP core−shell structure was constructed in the present work by considering the aspects of morphology and interfacial energetics for use as the photoelectrode of a PEC cell. A light harvest of more than 95% in the range of 300−375 nm was achieved using the hierarchical TiO_2 nanostructured photoelectrode with a thickness of ∼2 μm. The quasi-single-crystalline ND array with NPs in the shell portion provides a large surface area for efficient photocharge separation without significantly sacrificing the electron collection efficiency. Moreover, ANPs on the surface of the ND/RNP array enhance charge separation and suppress charge recombination at the interfacial region between the electrode and water due to the conduction band edge of anatase TiO_2 being higher than that of rutile TiO_2. Through both morphology and interfacial energetics controls for the PEC photoelectrode, a remarkable photocurrent density and the highest photoconversion efficiency of 2.08 mA cm^{-2} at 1.23 V vs RHE and 1.13% at 0.51 V vs RHE are, respectively, attained using the hierarchical TiO_2 nanostructured array PEC cell under illumination of AM 1.5G.

ASSOCIATED CONTENT

Supporting Information

Raman spectra and SEM images of the TiO_2 nanostructured array, EIS analyses of the characteristic times of electron transport through the TiO_2 photoelectrode and charge transfer at the interface, TEM image of NW/RNP, and SEM images of NW/RNP and ND/RNP arrays before and after the ANP growth. This information is available free of charge via the Internet at http://pubs.acs.org.

AUTHOR INFORMATION

Corresponding Author

*E-mail: wujj@mail.ncku.edu.tw.

Author Contributions

The manuscript was written through contributions of all authors. All authors have given approval to the final version of the manuscript.

Notes

The authors declare no competing financial interest.

ACKNOWLEDGMENTS

The financial support from the National Science Council of Taiwan under Grants NSC 99-2221-E-006-198-MY3 and NSC 100-2628-E006-032-MY2 is gratefully acknowledged.

REFERENCES

(1) Fujishima, A.; Honda, K. *Nature* **1972**, *238*, 37−38.
(2) Kudo, A.; Miseki, Y. *Chem. Soc. Rev.* **2009**, *38*, 253−278.
(3) Walter, M. G.; Warren, E. L.; McKone, J. R.; Boettcher, S. W.; Mi, Q.; Santori, E. A.; Lewis, N. S. *Chem. Rev.* **2010**, *110*, 6446−6473.
(4) Sivula, K.; Le Formale, F.; Grätzel, M. *ChemSusChem* **2011**, *4*, 432−449.
(5) Chen, X. B.; Shen, S. H.; Guo, L. J.; Mao, S. S. *Chem. Rev.* **2010**, *110*, 6503−6570.
(6) Chen, X. B.; Liu, L.; Yu, P. Y.; Mao, S. S. *Science* **2011**, *331*, 746−750.
(7) Maeda, K. *J. Photochem. Photobiol., C: Photochem. Rev.* **2011**, *12*, 237−268.
(8) Hanaor, D. A. H.; Sorrell, C. C. *J. Mater. Sci.* **2011**, *46*, 855−874.
(9) Kho, Y. K.; Iwase, A.; Teoh, W. Y.; Mädler, L.; Kudo, A.; Amal, R. *J. Phys. Chem. C* **2010**, *114*, 2821−2829.
(10) Chen, H. M.; Chen, C. K.; Liu, R. S.; Zhang, L.; Zhang, J.; Wilkinson, D. P. *Chem. Soc. Rev.* **2012**, *41*, 5654−5671.
(11) Takahashi, M.; Tsukigi, K.; Uchino, T.; Yoko, T. *Thin Solid Films* **2001**, *388*, 231−236.
(12) Zhang, Z.; Wang, P. *Energy Environ. Sci.* **2012**, *5*, 6506−6512.
(13) Cho, I. S.; Chen, Z. B.; Forman, A. J.; Kim, D. R.; Rao, P. M.; Jaramillo, T. F.; Zheng, X. L. *Nano Lett.* **2011**, *11*, 4978−4984.
(14) Hwang, Y. J.; Hahn, C.; Liu, B.; Yang, P. D. *ACS Nano* **2012**, *6*, 5060−5069.
(15) Liu, M. Z.; Snapp, N. D.; Park, H. *Chem. Sci.* **2011**, *2*, 80−87.
(16) Liao, W. P.; Wu, J. J. *J. Mater. Chem.* **2011**, *21*, 9255−9262.
(17) Lin, C. J.; Lu, Y. T.; Hsieh, C. H.; Chien, S. H. *Appl. Phys. Lett.* **2009**, *94*, 113102.
(18) Chen, H. M.; Chen, C. K.; Chang, Y. C.; Tsai, C. W.; Liu, R. S.; Hu, S. F.; Chang, W. S.; Chen, K. H. *Angew. Chem., Int. Ed.* **2010**, *49*, 5966−5969.
(19) Ng, Y. H.; Iwase, A.; Kudo, A.; Amal, R. *J. Phys. Chem. Lett.* **2010**, *1*, 2607−2612.
(20) Hagfeldt, A.; Lindström, H.; Södergren, S.; Lindquist, S.-E. *J. Electroanal. Chem.* **1995**, *381*, 39−46.
(21) Ku, C. H.; Wu, J. J. *Appl. Phys. Lett.* **2007**, *91*, 093117.
(22) Wong, D. K.-P.; Ku, C.-H.; Chen, Y.-R.; Chen, G.-R.; Wu, J.-J. *ChemPhysChem* **2009**, *10*, 2698−2702.
(23) Fujishima, A.; Zhang, X. T.; Tryk, D. A. *Surf. Sci. Rep.* **2008**, *63*, 515−582.
(24) Yamakata, A.; Ishibashi, T.-a.; Onishi, H. *J. Phys. Chem. B* **2001**, *105*, 7258−7262.
(25) Hoffmann, M. R.; Martin, S. T.; Choi, W. Y.; Bahnemann, D. W. *Chem. Rev.* **1995**, *95*, 69−96.
(26) Salvador, P. *J. Appl. Phys.* **1984**, *55*, 2977.